Proc. Natl. Acad. Sci. USA
Vol. 92, pp. 9707–9711, October 1995
Cell Biology

Kinetics of spindle pole body separation in budding yeast

JASON A. KAHANA*, BRUCE J. SCHNAPP†, AND PAMELA A. SILVER*‡

*Department of Biological Chemistry and Molecular Pharmacology, Harvard Medical School and Dana–Farber Cancer Institute, 44 Binney Street, Boston, MA 02115; and †Department of Cell Biology, Harvard Medical School, Boston, MA 02115

Communicated by Bruce M. Alberts, National Academy of Sciences, Washington, DC, July 17, 1995

ABSTRACT **In the budding yeast *Saccharomyces cerevisiae*, the spindle pole body (SPB) serves as the microtubule-organizing center and is the functional analog of the centrosome of higher organisms. By expressing a fusion of a yeast SPB-associated protein to the *Aequorea victoria* green fluorescent protein, the movement of the SPBs in living yeast cells undergoing mitosis was observed by fluorescence microscopy. The ability to visualize SPBs *in vivo* has revealed previously unidentified mitotic events. During anaphase, the mitotic spindle has four sequential activities: alignment at the mother–daughter junction, fast elongation, translocation into the bud, and slow elongation. These results indicate that distinct forces act upon the spindle at different times during anaphase.**

During mitosis, chromosome segregation is mediated by the mitotic spindle. The spindle consists of a network of interdigitating microtubules that emanate from a pair of microtubule-organizing centers (MTOCs). In the budding yeast *Saccharomyces cerevisiae*, the MTOC, termed the spindle pole body (SPB), remains embedded in the nuclear envelope as the cell undergoes a closed mitosis (1). Early in the cell division cycle, the single SPB moves toward the bud site and duplicates (2, 3). Near the end of S phase, the two SPBs move apart and form a short (≈1 μm) spindle. The short spindle then localizes to the mother–bud junction (termed the bud neck), and elongation commences.

The *NUF2* gene of yeast encodes a protein that localizes to the nuclear face of the SPB (4). Nuf2p contains a large segment of coiled-coil structure, and mutations in this region result in cells arrested with a shortened mitotic spindle and fully replicated DNA (4). Nuf2p is a particularly suitable marker for observing SPBs in living cells because it remains SPB-associated throughout the cell cycle, and it can be overexpressed without toxic side effects (4).

Because the mechanisms governing SPB movement have yet to be determined, we have developed an innovative strategy to observe its dynamics in living cells: visualization of a functional fusion between a SPB-associated protein and the *Aequorea victoria* green fluorescent protein (GFP) (5, 6). GFP has a number of advantages as a fluorescent reporter protein; in particular it requires no cofactor for visualization and can be expressed in a number of heterologous cell types (6).

MATERIALS AND METHODS

Plasmid Construction. Plasmid pKG5 was constructed as follows: wild-type GFP was PCR-amplified from plasmid TU 65 (5) using the 5′ *Xho* I-linked primer CCGCTCGAGCTATGAGTAAAGGAGAAGA and the 3′ T7 primer. The PCR product was cut with *Xho* I and *Pst* I (New England Biolabs). The NUF2 open reading frame was amplified from plasmid pPS511 (4) using the *Bam*HI-linked 5′ primer GCGGATCCATGAGTAGGAATCAAGATGTC and the in-frame, *Xho* I-linked 3′ primer CCCTCGAGCTTGCATATATTCGAGCAT. The PCR product was cut with *Bam*HI and *Xho* I. The two fragments were ligated together into plasmid pPS293 (a 2-μm URA3 vector with the *GAL1* promoter sequence) cut with *Bam*HI and *Pst* I.

Plasmid pJK6 was constructed as follows: Plasmid pPS511 was cut with *Bam*HI and *Nhe* I. A 359-bp fragment encompassing the *NUF2* 5′ promoter region along with the first 78 nucleotides of the coding sequence was isolated. This fragment was ligated into a pKG5 backbone, which had been cut with *Bam*HI and *Nhe* I. This resulted in a 2-μm vector, which had the *GAL1* promoter upstream of the *NUF2* promoter and the *NUF2–GFP* coding sequence.

Western Blots. Whole cell extracts were prepared by suspending 1–3 × 10^8 cells in 200 μl of protein sample buffer (7) with glass beads, followed by agitation and heating at 95°C for 5 min. Ten microliters of each extract was run on a SDS/10% polyacrylamide gel, transferred to nitrocellulose, and probed with 1:2000 anti-Nuf2p rabbit polyclonal antibody (4) followed by 1:4000 horseradish peroxidase-conjugated anti-rabbit IgG (Promega). Blots were then visualized by using ECL detection reagents as directed by the manufacturer (Amersham).

Visualization of SPBs in Living Cells. Diploid strain PSY630 cells (*Matα/a; ura3-52/ura3-52; leu2Δ1/leu2Δ1; trp1Δ63/TRP1; his3Δ200/HIS3; NUF2/NUF2*) transformed with pJK6 were grown at 30°C in SC −ura medium (8) supplemented with 2% glucose to a density of 5 × 10^6 cells per ml, collected by centrifugation, resuspended in YPD medium (8), and incubated at 30°C for 30–60 min. Three microliters was placed on a microscope slide, covered with a coverslip (22 × 22 mm), sealed with Valap wax, and grown at 30°C until buds were 40–50% the length of their mothers (35–40 min). Partial depletion of the oxygen from the medium by the cells may reduce the amount of photodamage to the cells during fluorescence observations. The cells were then observed by fluorescence with a CH250/KAF-1400 liquid-cooled CCD camera (Photometrics, Tucson, AZ) on a Zeiss Axioskop equipped with the following filter set: excitation, 465–495 nm; dichroic, 510 nm; barrier, 520 LP (Chroma Technology, Brattleboro, VT), a 200-W mercury arc lamp (Opti-Quip), and a ×63 1.4 numerical aperture Plan-Apochromat objective. The final magnification to the CCD array was ≈×75; that is, 1 μm (of the specimen) projected onto 11 pixels of the CCD array where each pixel is 6.8 × 6.8 μm. The quantum efficiency of the KAF-1400 CCD chip is rated at ≈30% at the emission maximum (509 nm) of GFP. Excitation illumination was controlled by an integrated shutter (Uniblitz, Rochester, NY) synchronized with the digital camera. Cells were observed using 500-ms exposures at 10-s intervals with manually controlled motorized focusing (Ludl). Digitized images were acquired using the MetaMorph imaging system (Universal Imaging, Media, PA).

The distance between SPBs was measured using the measure distance feature of the METAMORPH imaging software (Universal Imaging) calibrated to a 10-μm stage micrometer.

The publication costs of this article were defrayed in part by page charge payment. This article must therefore be hereby marked "*advertisement*" in accordance with 18 U.S.C. §1734 solely to indicate this fact.

Abbreviations: SPB, spindle pole body; GFP, green fluorescent protein.

‡To whom reprint requests should be addressed.

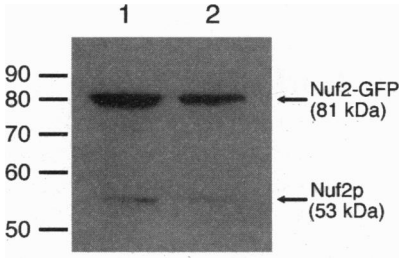

FIG. 1. Immunoblot analysis of Nuf2p and Nuf2–GFP expression in yeast cells. Cell extracts from strain PSY630 (*Matα/a; ura3-52/ura3-52; leu2Δ1/leu2Δ1; trp1Δ63/TRP1; his3Δ200/HIS3; NUF2/NUF2*) harboring pJK6 encoding Nuf2–GFP under control of the *NUF2* promoter on a 2-μm (multicopy) plasmid (lane 1) or pJK5 encoding Nuf2–GFP under control of the *GAL1* promoter with (lane 2) 1 hr of galactose induction and 6 hr of glucose chase were probed with anti-Nuf2p polyclonal antibody. Nuf2–GFP migrates at the predicted molecular mass of 81 kDa. In calibrated immunoblot experiments, we observed that galactose pulse–chase expression results in a 2- to 4-fold higher level of expression, while constitutive expression of Nuf2–GFP from a high-copy plasmid results in a level of protein 4- to 5-fold higher than that provided from the chromosomal copies of *NUF2* (results not shown).

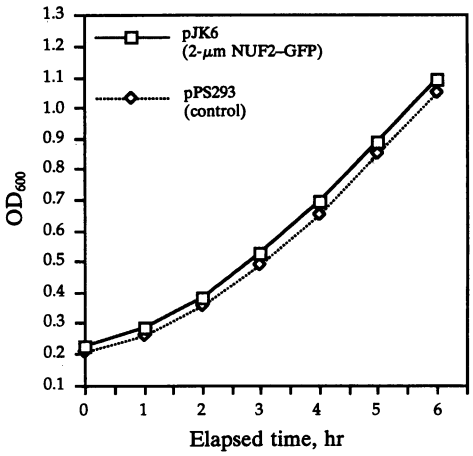

FIG. 2. Growth rates of Nuf2–GFP-expressing and control cells. The growth rate of Nuf2–GFP-expressing cells is indistinguishable from that of cells harboring a control plasmid. Diploid PSY630 cells transformed with pJK6 and pPS293 (2-μm plasmid lacking the *NUF2–GFP* gene) were grown at 30°C in SC −ura medium supplemented with 2% glucose (8), and the OD_{600} of the culture was measured at 1-hr intervals.

Rate measurements were taken only if the two SPBs appeared parfocal within a particular frame. All distances are measured from the centers of the fluorescent regions. Average fast elongation rates were measured for 10 different experiments using available parfocally measured distances.

For galactose-induced expression (9), PSY630 cells transformed with pJK5 were grown in SC −ura supplemented with 2% raffinose at 30°C to a density of 2–5 × 10^6 cells per ml. Galactose was added to a final concentration of 2%, and the cells were incubated for 1 hr at 30°C. The cells were then centrifuged and resuspended in SC −ura supplemented with 2% glucose. The cells were grown for 6 hr at 30°C and then observed by epifluorescence microscopy.

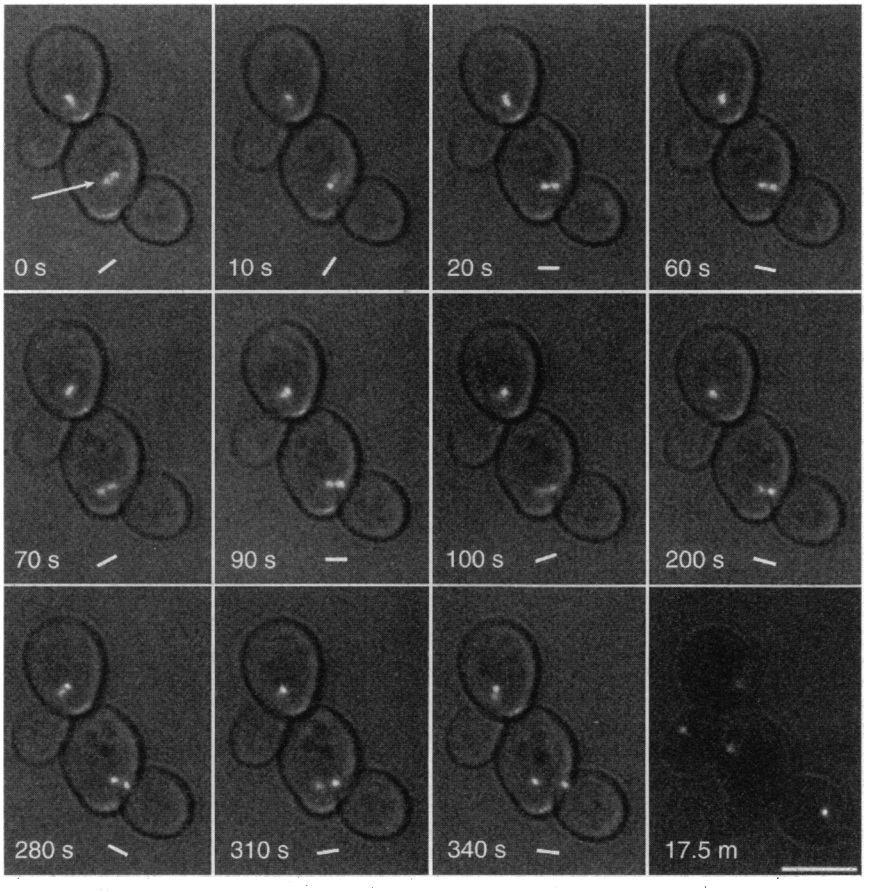

FIG. 3. Random changes in orientation of the short spindle during alignment at the mother–bud junction. Nuf2–GFP at the SPBs (arrow) was observed by epifluorescence microscopy with low bright-field illumination. Elapsed time is shown in each panel; short line indicates orientation of the spindle. Final frame (17.5 min) confirms that these cells completed anaphase. Progress of bud growth during irradiation with excitation illumination is indistinguishable from that of unirradiated cells as observed by differential interference contrast (DIC) microscopy. Random oscillations were observed in all seven experiments in which observations were initiated before the fast elongation phase. (Bar = 5 μm.)

RESULTS

We constructed two yeast expression plasmids that encode GFP fused to the C terminus of Nuf2p. Antibodies against Nuf2p recognize both the endogenous Nuf2p as well as the GFP fusion of predicted molecular masses from extracts of cells harboring Nuf2–GFP expression constructs (Fig. 1).

As observed by standard epifluorescence microscopy, the Nuf2p–GFP fusion protein localizes at the SPB in a manner indistinguishable from that of wild-type Nuf2p, whereas native GFP is uniformly distributed throughout the yeast cell (results not shown). To visualize the SPBs by epifluorescence microscopy (see Figs. 3–5), a level of Nuf2–GFP expression 2- to 5-fold higher than that produced by the endogenous *NUF2* promoter is required. At this level of Nuf2–GFP expression, the SPB can be visualized by eye using a ×63 objective/×10 eyepiece with a 50-W mercury epifluorescence illuminator. Based on calibrated immunoblots, we estimate that there are between 2500 and 10,000 Nuf2–GFP molecules per cell (results not shown).

Overexpression of Nuf2–GFP had no effect on the growth rate of cells compared to their nonexpressing counterparts (Fig. 2). Moreover, overexpression of Nuf2–GFP completely restores growth at 37°C to strains harboring the conditional lethal *nuf2-61* allele, indicating that it is functional. Thus, expression of the Nuf2–GFP fusion protein from the inducible *GAL1* promoter (9) or from a multicopy plasmid provided us with a fluorescent tag for the SPB *in vivo*.

The observations reported here are focused on a 15- to 30-min period from the localization of the short spindle at the bud neck through the breakdown of the elongated spindle. We observed that prior to elongating, the short spindle undergoes a series of seemingly random motions before localizing at, or slightly through, the bud neck (Fig. 3). During this period, the spindle becomes displaced in both angular orientation and position until it is properly aligned at the bud neck along the mother–bud axis. Notably, the short spindle does not begin elongating immediately after alignment; it may move away and reposition itself several times (Fig. 3, 20–90 s) before elongation actually commences (Fig. 3, 280–310 s). Furthermore, the orientation of the spindle does not necessarily remain static during elongation; we typically observed small (<20°) changes in orientation once elongation had begun (Fig. 3, 310–340 s). However, we never observed elongation of a spindle that was grossly misoriented or not localized to the mother–bud junction in wild-type cells (n = 12). Thus, the positioning of the spindle occurs both before and during elongation and involves a variety of ostensibly random movements.

Within 30 s of finding its final proper orientation, the SPBs separate at an average rate of 1.48 μm/min (n = 10; SD = 0.114 μm/min) over a period of 100–150 s (Fig. 4). We refer to this as fast elongation. During this period of time, the position of the daughter's SPB is relatively fixed within a 0.5-μm radius of the mother–bud junction such that the spindle appears to elongate mainly within the mother cell. Furthermore, the elongation rate is roughly constant over the entire period of fast elongation when measured at 10-s intervals (Fig. 4).

Once the spindle has grown to 50–60% the length of the mother, the entire spindle translocates as a unit into the daughter cell (Fig. 4, 110–150 s; Fig. 5*A*). In Fig. 5*A*, the daughter's SPB is displaced 1.7 μm over a period of 70 s, although the spindle elongated only 0.30 μm. Therefore, the entire spindle was displaced at least 1.3 μm. Thus, there exists an activity distinct from elongation, which contributes to the movement of the daughter's SPB into the bud. Although we have observed that translocation may coincide with a temporary arrest in elongation (Fig. 5 *A* and *C*), we have also noticed that translocation may initiate while fast elongation is still occurring (Fig. 4, 110–150 s). It has been previously shown that when cells are transiently arrested before anaphase with hydroxyurea or a *cdc16-2* temperature-sensitive mutation, short spindles are capable of traversing the bud neck upon return to permissive conditions (10, 11). Our findings indicate that translocation of the elongated spindle is a part of normal mitosis in wild-type cells.

After translocation, the spindle continues to elongate over 10–12 min until the SPBs are at the distal ends of the mother and daughter (Fig. 5*B*). However, the rate of elongation during this period is markedly slower than that of the fast elongation phase. We observed that the average rate of this slow elongation was 0.69 μm/min (n = 7; SD = 0.138 μm/min), roughly half that of fast elongation. During this period of time, the separated SPBs continue to move coordinately, indicating that they are still connected by a mobile spindle (Fig. 5*B*). Once slow elongation has ceased, the breakdown of the anaphase

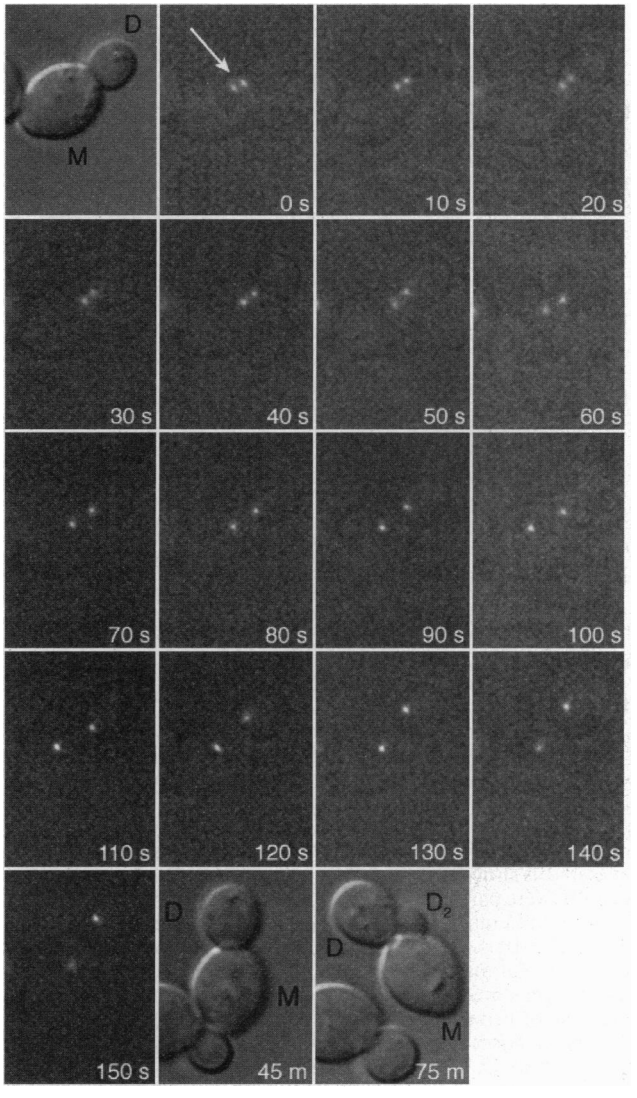

FIG. 4. Fast elongation of the mitotic spindle. Note that the parfocality of the stained regions (arrow) indicates that the spindle is oriented parallel to the plane of focus. Elapsed time is indicated in each frame. First frame is a differential interference contrast (DIC) microscopy image of the cells before fluorescence observations were initiated. Final two frames show that the cells continue to divide after observations were made. Note that the cells have shifted position during observations (M, mother cell; D, daughter; D_2, mother's second bud). Over any 10-s interval during the fast elongation step, the average elongation rate for this particular spindle was 1.61 μm/min (n = 10; SD = 0.198 μm/min).

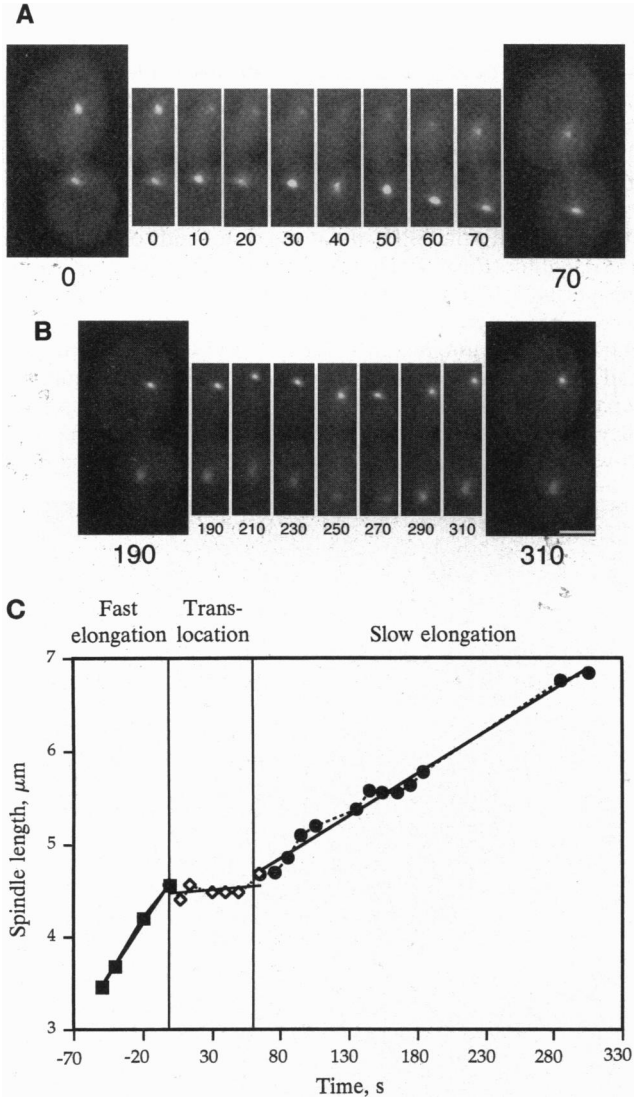

FIG. 5. Translocation followed by slow elongation. (*A*) After the period of fast elongation, the spindle translocates into the daughter cell. Mother (upper) and daughter (lower) cells are shown at $t = 0$ and $t = 70$ s. Spindle regions are shown over the entire 70-s interval. This phenomenon was observed in all seven experiments in which both SPBs remained in focus during the period immediately after fast elongation. (Bar = 2 μm.) (*B*) Slow elongation of the mitotic spindle. Same mother and daughter are shown after translocation at $t = 190$ and $t = 310$ s. The spindle regions are shown over the entire 120-s interval. For this experiment, the slow rate was 0.65 μm/min when measured as an average of nine intervals (SD = 0.13 μm/min) in which the SPBs were parfocal. Average slow elongation rates were measured for seven different experiments using available parfocally measured distances. After observations, both the mother and daughter cells underwent mitosis twice within 4 hr. (*C*) Graph of spindle length vs. time for cells in *A* and *B*. Parfocal distances were measured, and a linear curve fit was computed for each phase using CRICKET GRAPH (Computer Associates). Based on the slopes of the three lines, fast elongation (−70 to 0 s) for this spindle occurred at 1.32 μm/min. During translocation (0–70 s), the rate of elongation was ≈0.06 μm/s. Slow elongation occurred at ≈0.58 μm/min.

spindle is apparent when the SPBs begin to move independently of one another (results not shown).

DISCUSSION

In summary, the observations of Nuf2–GFP reported here allow us to dissect spindle dynamics during anaphase into four activities: alignment, fast elongation, translocation, and slow elongation (e.g., see Fig. 5*C*). Nuf2–GFP is functional and cell division continues at a normal pace throughout the course of these experiments. Based on these criteria, the kinetics of SPB separation we report most likely represent the course of normal anaphase.

Astral microtubules (11), the actin cytoskeleton (11), dynactin complex proteins (12, 13), and cytoplasmic dynein (14, 15) have all been shown to have roles in proper spindle positioning in yeast. During development of multicellular organisms, spindle orientation plays an important role in positioning of adjacent cells (16, 17). Since cytoplasmic dynein has been localized to the mitotic spindle of mammalian and avian cells (18, 19), the mechanism of spindle alignment at the yeast bud neck may be similar to that of metazoan spindle orientation.

The existence of two distinct rates of spindle elongation at different times during anaphase (Fig. 5*C*) suggests that there are distinct sets of forces that contribute to spindle extension. It has been previously shown that two kinesin-like proteins, Cin8p and Kip1p, are involved in spindle elongation during anaphase and have apparently redundant functions (20–22). Our results suggest that different forces appear to act on the spindle at different times during anaphase. Notably, the fast elongation step appears to take place while the spindle growth is confined within the mother cell while slow elongation occurs after the spindle has translocated through the bud neck. Consequently, a signal may link translocation with the transition from fast to slow elongation.

The ability to visualize the spindle poles during cell division in intact cells is a powerful tool for identification of forces active during mitosis. Since *S. cerevisiae* is a genetically tractable organism used in the study of cell division, *in vivo* visualization of the SPBs will be a useful technique for determining the precise effects of mutations in genes that affect chromosome segregation and the progression of the cell cycle. Furthermore, identification of the various movements of the spindle during mitosis should aid in the isolation of genes responsible for proper spindle function during polarized cell division in yeast and higher eukaryotes.

Note Added in Proof. Similar findings have recently been reported by Yeh *et al.* (23).

We thank David Pellman for helpful discussions and comments on the manuscript. This work was supported by National Institutes of Health grants to P.A.S. and B.J.S. and by a Claudia Adams Barr Investigatorship to P.A.S. J.A.K. was supported by National Institutes of Health training grants to Harvard University and Harvard Medical School and by a Mazur Foundation fellowship.

1. Moens, P. B. & Rappaport, E. (1971) *J. Cell Biol.* **50,** 344–361.
2. Byers, B. & Goetsch, L. (1974) *Cold Spring Harbor Symp. Quant. Biol.* **38,** 123–131.
3. Byers, B. & Goetsch, L. (1975) *J. Bacteriol.* **124,** 511–533.
4. Osborne, M. A., Schlenstedt, G., Jinks, T. & Silver, P. A. (1994) *J. Cell Biol.* **125,** 853–866.
5. Prasher, D. C., Eckenrode, V. K., Ward, W. W., Prendergrast, F. G. & Cormier, M. J. (1992) *Gene* **111,** 229–233.
6. Chalfie, M., Tu, Y., Euskirchen, G., Ward, W. W. & Prasher, D. C. (1994) *Science* **263,** 802–805.
7. Sambrook, J., Fritsch, E. F. & Maniatis, T. (1982) *Molecular Cloning: A Laboratory Manual* (Cold Spring Harbor Lab. Press, Plainview, NY).
8. Sherman, F. (1991) *Methods Enzymol.* **194,** 3–21.
9. Yocum, R. R., Hanley, S., West, R. & Ptashne, M. (1984) *Mol. Cell. Biol.* **4,** 1985–1998.
10. Palmer, R. E., Koval, M. & Koshland, D. (1989) *J. Cell Biol.* **109,** 3355–3366.
11. Palmer, R. E., Sullivan, D. S., Huffaker, T. & Koshland, D. (1992) *J. Cell Biol.* **119,** 583–593.
12. Clark, S. W. & Meyer, D. I. (1994) *J. Cell Biol.* **127,** 129–138.
13. Muhua, L., Karpova, T. S. & Cooper, J. A. (1994) *Cell* **78,** 669–679.

14. Li, Y.-Y., Yeh, E., Hays, T. & Bloom, K. (1993) *Proc. Natl. Acad. Sci. USA* **90,** 10096–10100.
15. Eshel, D., Urrestarazu, L. A., Vissers, S., Jauniaux, J.-C., van Vliet-Reedijk, J. C., Planta, R. J. & Gibbons, I. R. (1993) *Proc. Natl. Acad. Sci. USA* **90,** 11172–11176.
16. Hyman, A. A. & White, J. G. (1987) *J. Cell Biol.* **105,** 2123–2135.
17. Hyman, A. A. (1989) *J. Cell Biol.* **109,** 1185–1193.
18. Pfarr, C. M., Coue, M., Grissom, P. M., Hays, T. M., Porter, M. E. & McIntosh, J. M. (1990) *Nature (London)* **345,** 263–265.
19. Steuer, E. R., Wordeman, L., Schroer, T. A. & Sheetz, M. P. (1990) *Nature (London)* **345,** 266–268.
20. Hoyt, M. A., He, L., Loo, K. K. & Saunders, W. S. (1992) *J. Cell Biol.* **118,** 109–120.
21. Saunders, W. S. & Hoyt, M. A. (1992) *Cell* **70,** 451–458.
22. Roof, D. M., Meluh, P. B. & Rose, M. D. (1992) *J. Cell Biol.* **118,** 95–108.
23. Yeh, E., Skibbens, R. V., Cheng, J. W., Salmon, E. D. & Bloom, K. (1995) *J. Cell Biol.* **130,** 687–700.